# AUTHOR QUERIES

# AUTHOR PLEASE ANSWER ALL QUERIES

**PLEASE NOTE: We cannot accept new source files as corrections for your article. If possible, please annotate the PDF proof we have sent you with your corrections and upload it via the Author Gateway. Alternatively, you may send us your corrections in list format. You may also upload revised graphics via the Author Gateway.**

**Carefully check the page proofs (and coordinate with all authors); additional changes or updates WILL NOT be accepted after the article is published online/print in its final form. Please check author names and affiliations, funding, as well as the overall article for any errors prior to sending in your author proof corrections. Your article has been peer reviewed, accepted as final, and sent in to IEEE. No text changes have been made to the main part of the article as dictated by the editorial level of service for your publication.**

AQ:1 = Please confirm or add details for any funding or financial support for the research of this article.

AQ:2 = Please provide the full current affiliation details (department name, name of university/institution, city, state/country, and zip/postal code) for all the authors.

IEEE Proof

# Dynamic Nonlinear Resistance Model for a Power MOSFET in an Oscillatory RLC Circuit

Soniya Raju, *Member, IEEE*, D. Alistair Steyn-Ross, Marcus Wilson, and Nihal Kularatna, *Senior Member, IEEE*

IEEE Proof

***Abstract*—This paper presents the development of a new MATLAB MOSFET model specifically designed for RLC circuits. The key contribution is the formulation of a novel equation that accurately captures the device behavior across subthreshold, above-threshold regions and at threshold point, addressing limitations in existing models. The developed model treats the MOSFET as a variable resistance element, with the resistance changing dynamically at each instant, enabling the solution of differential equations governing the RLC circuit. Curve fitting and refinement were conducted based on experimental results, leading to a close match between the simulations and experimental data. The model was tested with triangle, sinusoidal and quadrilateral gate voltages, and the simulation results show good match with the experimental data, demonstrating the model's accuracy. It provides a straightforward way to predict performance, making it easier to refine and optimize the design gate voltage before physical implementation. This work provides a solid foundation for MOSFET modeling in oscillatory RLC circuits, which can be applied to a wide range of power electronics applications.**

***Index Terms*—Supercapacitors, transcranial magnetic stimulation (TMS), power semiconductor switches, pulse generator, magnetic stimulation, pulse circuits, nonlinear MOSFET model.**

## I. Introduction

METAL-OXIDE semiconductor field effect transistor (MOSFET) models play a crucial role in simulating and understanding device behavior in power electronics. Various MOSFET models have been developed to accurately represent their characteristics in circuit simulations. These models fall into three broad categories: physics-based, analytical, and behavioral. Physics-based models, often used in technology computer-aided design (TCAD) simulations, focus on detailed internal phenomena such as electron mobility, channel length modulation, and threshold voltage shifts. While these models offer high accuracy, they can be computationally intensive and difficult to use for practical applications in power circuits due to the complexity of the physical phenomena being modeled [1], [2]. Analytical models, such as the Unified Charge Control Model (UCCM), rely on mathematical expressions to describe device behavior and to provide a clear relationship between key parameters like current, transconductance, and threshold voltage. Though more efficient for simulations than physics-based models, they can become complicated when high accuracy is required [3], [4].

Behavioral models, including widely-used SPICE models, are designed to simplify the simulation of MOSFETs for practical applications like power converters, automotive systems, and switching devices. These models focus on representing the overall electrical behavior of the MOSFET rather than the internal physical details. SPICE models are generally preferred for applications requiring fast and efficient simulation because they strike a balance between accuracy and simplicity. A SPICE model for a 6.5 kV SiC MOSFET was recently developed to closely match the device's static and dynamic characteristics, demonstrating how behavioral models can still achieve reasonable accuracy for power applications [5]. While behavioral models are simpler and more user-friendly, they can lack the precision needed for complex scenarios, particularly where parasitic elements (stray inductance and capacitance) or extreme operating conditions such as high switching frequencies or elevated temperatures come into play.

One of the major challenges in MOSFET modeling is the accurate simulation of switching behavior and parasitic effects. SiC MOSFETs offer lower on-state resistance than traditional silicon MOSFET, higher breakdown voltages, and faster switching speeds, making them suitable for high-voltage and high-frequency applications [6]. While several models have been proposed for SiC MOSFETs, such as the Hefner model and its derivatives [7], these models often require extensive parameter extraction from datasheets or experimental data, limiting their practical use in everyday circuit design. A recent approach involves using a modified Enz-Krumenacher-Vittoz (EKV) model [8] for SiC MOSFETs, which offers a single equation for the entire operating range, from weak to strong inversion. This model has been successfully applied to simulate SiC MOSFETs in high-frequency switching applications, with validation against experimental data.

Several studies have focused on modeling SiC power devices. PSpice is widely used for SiC MOSFET modeling, but its limitations in handling complex equations can affect accuracy [8]. MATLAB/Simulink, with superior simulation and data processing capabilities, offers an alternative. Tornello et al. [9] developed an analytical model for single and parallel SiC configurations, achieving accurate

AQ:1 Received 27 November 2024; revised 26 January 2025; accepted 13 February 2025. This article was recommended by Associate Editor V. Lanza. *(Corresponding author: Soniya Raju.)*

AQ:2 The authors are with ??? (e-mail: sr231@students.waikato.ac.nz).

Digital Object Identifier 10.1109/TCSI.2025.3542754

1549-8328 © 2025 IEEE. All rights reserved, including rights for text and data mining, and training of artificial intelligence and similar technologies. Personal use is permitted, but republication/redistribution requires IEEE permission. See https://www.ieee.org/publications/rights/index.html for more information.

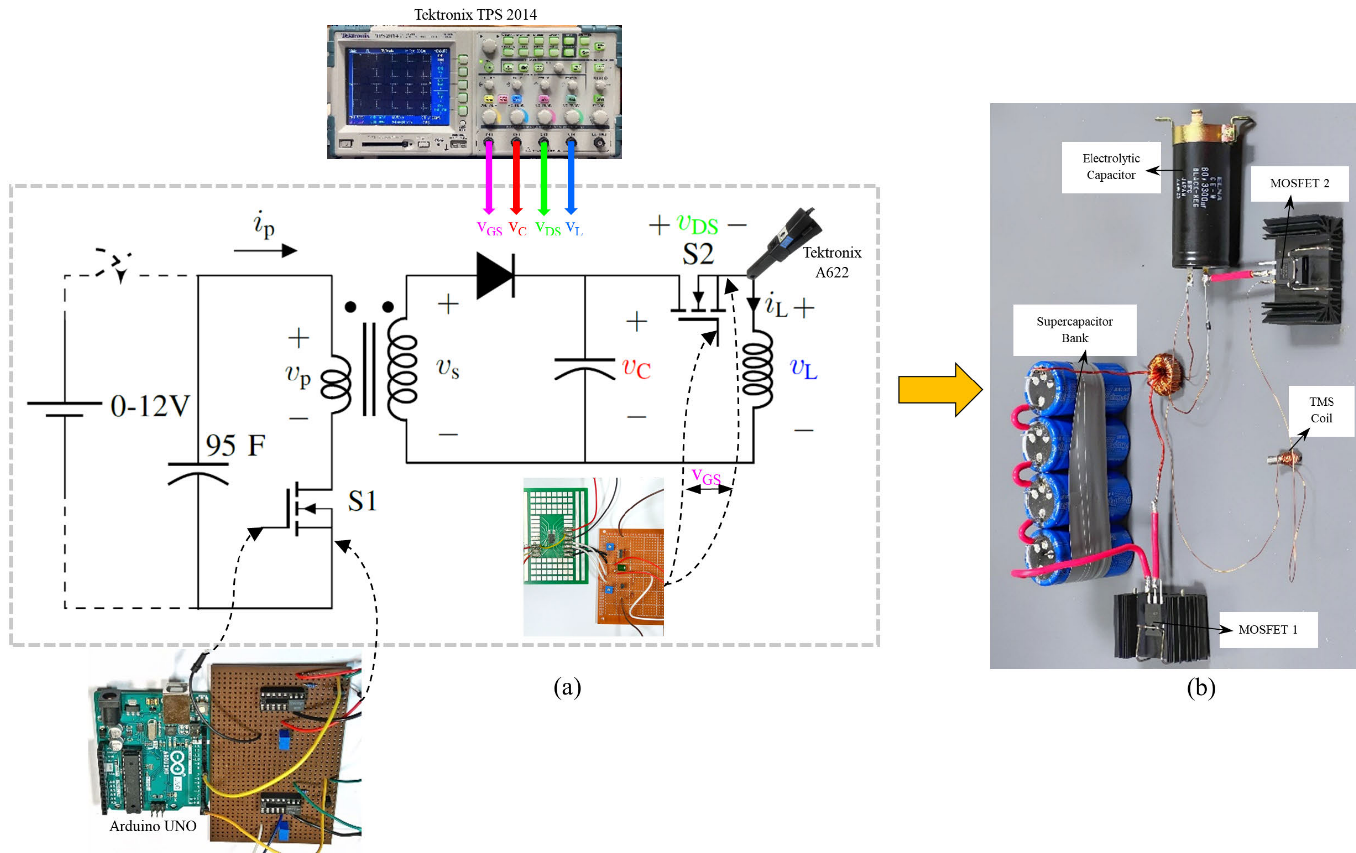


Fig. 1. Proof-of-concept prototype. Gate control signals for MOSFET S1 and S2 ensure that these switches are never ON at the same time. (a) Overall system with photos inserted showing external drivers to S1 from Arduino processor board, gate-drive waveform generator for S2 and oscilloscope; (b) experimental power stage.

switching transient behavior and energy loss predictions compared to SPICE models using 2D and 1D Look-Up Tables (LUTs) for device characteristics. Ferretti et al. [10] implemented a MATLAB-based approach to create I-V-T maps (lookup tables), including operating regions not covered in datasheets. Zeng et al. [11] conducted modeling research on parasitic capacitances ($C_{ds}$) and ($C_{gd}$) using MATLAB Simulink, extracting values from datasheets and curve-fitting for accuracy. While these studies relied on datasheet-based modeling and simulation, none explored the internal MOSFET variations, such as dynamic resistance changes, highlighting a gap in the current research.

Wang et al. [12] proposed a modeling method using PSpice with a dual voltage-dependent lookup table approach based on the envelope of the switching trajectory. Their method defines the value ranges for gate-source voltage ($v_{GS}$) and drain-source voltage ($v_{DS}$) during interterminal capacitance operation periods, considering only essential data within the switching trajectory and discarding unnecessary information outside it. Talesara et al. [13] implemented an analytical subcircuit model for SiC MOSFETs into Synopsys Saber [14], validating it against measured DC characteristics. They employed distinct equations for sub-threshold and threshold regions instead of a unified equation and used a Simulink-based approach rather than a purely mathematical one. Yang et al. [15] employ small-signal oscillations, utilizing linear analysis without attempting to model the actual switching phase transition.

Despite these advancements, existing MOSFET models still face limitations when applied in circuit simulations, particularly in power electronics. Many models are either too complex for practical use or fail to accurately match experimental results, especially in scenarios involving parasitic inductance and capacitance, which are common in power circuits. Engineers often encounter difficulties when trying to use off-the-shelf MOSFETs for which detailed models are unavailable. For instance, while several SiC MOSFET models, such as the Hefner model and SPICE models, are available, they often require complex parameter extraction processes and do not always capture all the physical phenomena that occur at different operating temperatures or switching speeds [16]. This highlights the need for a more simplified and generalized MOSFET model that can closely match experimental data without the need for extensive parameter tuning.

This paper aims to address this gap by proposing a new MOSFET model, developed in MATLAB, which is based on experimental results and tailored for use in electrical RLC circuits as first trial step. The model introduces a new equation that simplifies the representation of MOSFET behavior, focusing on the static and dynamic characteristics that are critical for power electronics applications. Unlike existing models that are either overly complex or limited in

their accuracy, this model is designed to be easy to implement while maintaining close alignment with experimental results. This approach offers a practical solution for engineers looking to simulate MOSFETs in power converters, motor controllers, and other high-voltage applications, where both accuracy and simplicity are essential. By bridging the gap between detailed physics-based models and simplified behavioral models, the proposed model provides a more balanced solution for modern power electronics design [5], [6], [8], [16], [17].

This paper details the development of a MATLAB simulation to model a MOSFET, enabling predictions of its behavior and the output of an RLC circuit. This RLC circuit is integral to the supercapacitor-based TMS pulse generator [18], which has been developed and successfully tested. To advance the design further, a simulation model was essential to verify output pulses, perform precise pulse shaping, and assess the impact of varying gate voltages on TMS pulse characteristics. However, no existing MOSFET equation or model was suitable for this application, prompting us to derive a new equation and create a MATLAB MOSFET model tailored for in-depth analysis. The process begins with an overview of the background study conducted for modeling, followed by modifications to existing equations to ensure proper functionality within the circuit. The creation of the MATLAB model is then described, based on experimental data, resulting in a complete MOSFET simulation model capable of predicting output current and voltage as functions of time, in response to gate voltage input. Finally, a comparison between the modeling and experimental results for a different scenario is presented. This study presents a solution applicable to any oscillatory RLC circuit incorporating a MOSFET, offering insights and modeling techniques beneficial for a range of applications beyond TMS pulse generation.

## II. Expression for Drain Current

Figure 1 shows the overall system, including the circuit diagram of the TMS pulse generator setup. This pulse generator [18] incorporates an RLC circuit in the final stage to excite the TMS coil. We developed this MOSFET model as part of our research study focused on pulse shaping capabilities and predicting the output TMS pulse. In this section, we discuss the modeling of the RLC part alone for a generic study.

Consider an RLC circuit containing an embedded MOSFET to control oscillatory current as shown in Fig. 2. We explicitly include the internal resistances of the capacitor ($r_C$) and the inductor ($r_L$).

Applying Kirchhoff's voltage law to Fig. 2,

$$v_C = v_L + (r_L + r_C + r_{DS}) i_L \quad (1)$$

where the ideal inductor voltage is given by $v_L = L\frac{di_L}{dt}$

Equation (1) can be rewritten as a first-order differential equation,

$$\frac{di_L}{dt} = \frac{1}{L}\left[v_C - (r_L + r_C + r_{DS}) i_L\right] \quad (2)$$

Thus if we know $r_{DS}$, we can numerically integrate Eq. (2) to find $i_L(t)$.

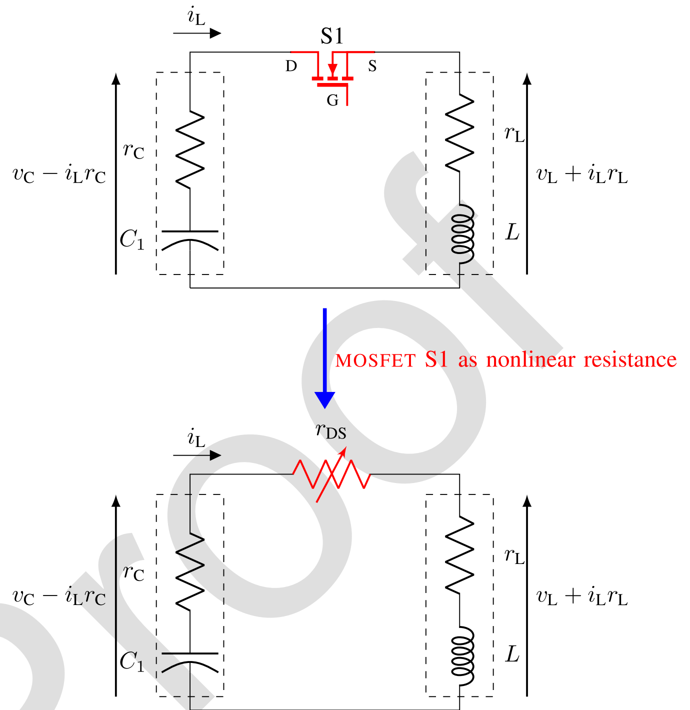


Fig. 2. The circuitry illustrates a RLC circuit, featuring the electrolytic capacitor $C_1$ along with its internal resistance $r_C$ feeding an inductive load characterized by an inductance $L$ and its internal resistance $r_L$. It includes a MOSFET switch represented as a nonlinear resistance $r_{DS}$, which depends on the gate-source voltage.

In these equations, we do not consider the MOSFET as a typical switching component. Instead, it is treated as an analog device, which behaves like a variable resistor controlled by the voltage applied to the gate. The challenge is to determine the time-varying resistance of the MOSFET as a function of input gate voltage for incorporation into differential equation (2).

By controlling the gate voltage $v_{GS}$, a MOSFET can be operated in distinct regions as shown in Fig. 3(a): subthreshold ($v_{GS} < v_T$), and above-threshold ($v_{GS} > v_T$). When gate voltage exceeds threshold, the MOSFET output characteristics moves from linear to saturation mode as $v_{GS}$ increases. Our focus is on developing a unified description for MOSFET behavior that encompasses transition through threshold.

### A. Subthreshold ($v_{GS} < v_T$)

In the subthreshold region, also known as the weak/cutoff region, the transistor remains in an 'off' state with minimal conduction. The small current flow into the drain is described by an exponential function of $v_{GS}$:

$$i_D \approx i_{D0} \exp\left(\frac{v_{GS} - v_T}{\eta\ v_{Th}}\right) \quad (3)$$

where applied gate voltage ($v_{GS}$), threshold voltage ($v_T$), thermal voltage ($v_{Th}$), and a subthreshold ideality factor ($\eta$) is used. The ideality factor accounts for the subthreshold division of the applied voltage between the gate insulator and the depletion layer [20].

IEEE Proof

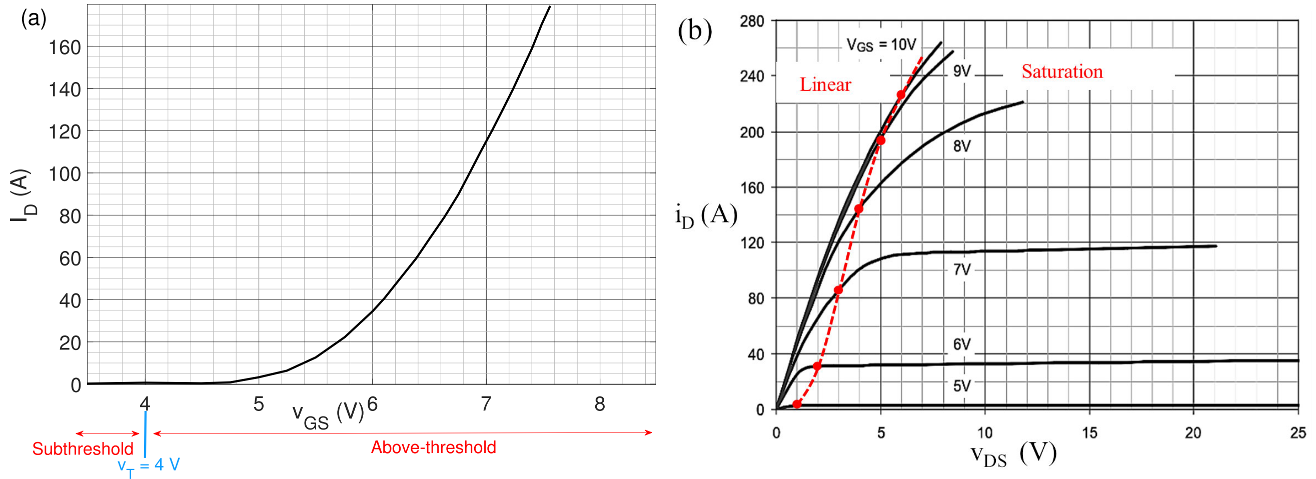


Fig. 3. (a) Drain current ($I_D$) against gate-source voltage ($v_{GS}$) of 25 °C and (b) drain current against the drain–source voltage for various gate voltages for MOSFET IXFK120N65 × 2 from data-sheet [19].The red dotted line in (b) indicates the above-threshold separation between linear and saturation modes, corresponding to $v_{DS}$ being less or greater than ($v_{GS} - v_T$) respectively. The threshold voltage ($v_T$) is set to 4 V here for demonstration, as the datasheet specifies a range for $v_T$ between 3 and 6 V.

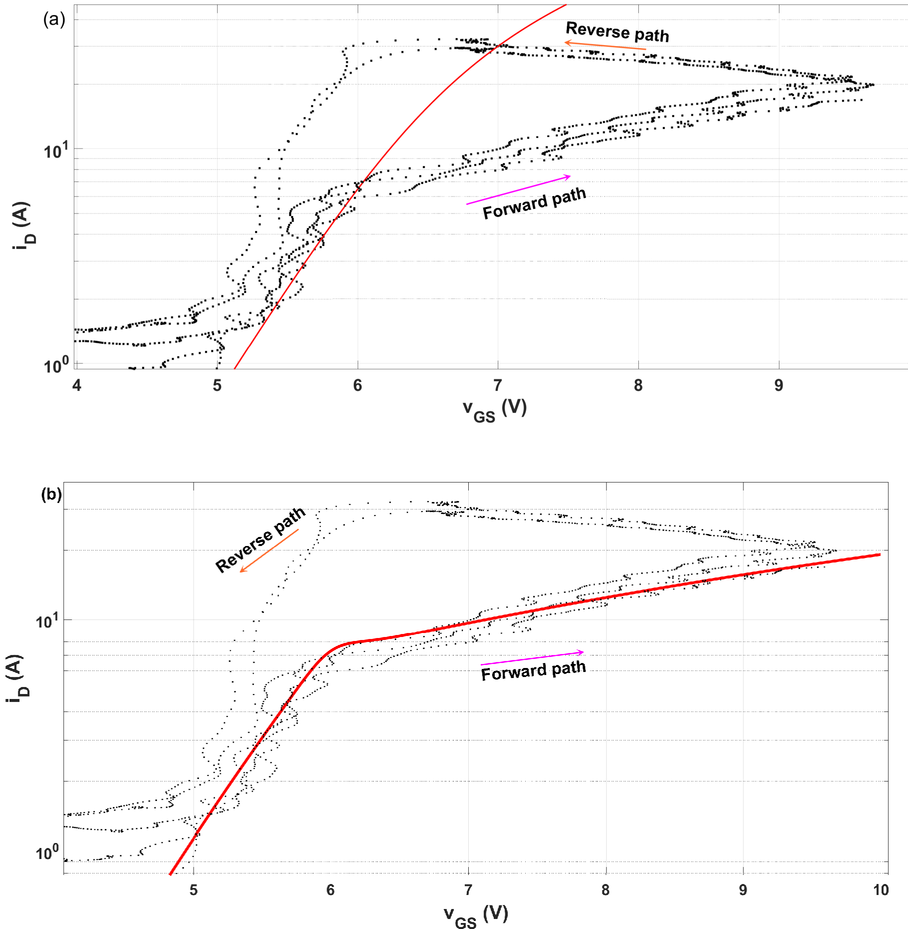


Fig. 4. (a) Curve fit (red line) for the MOSFET drain current $i_L$ for data points (black dots) from experiment using Eq. (7) which failed to fit; (b) improved curve using equation Eq. (15), provided a good match for the forward-path measurements.

### *B. Above Threshold ($v_{GS} > v_T$)*

In the above-threshold region, there are two operation modes depending on the drain-current characteristic with respect to drain-source voltage as in Fig 3(b). These are linear (also referred to as triode or ohmic), and saturation modes.

1) Linear mode ($v_{GS} > v_T, v_{DS} < (v_{GS} - v_T)$), the transistor activates, creating a narrow channel for current

to flow from drain to source. This region operates like a resistor, its conductance controlled by the gate-source voltage. The drain current in linear/ohmic mode consists of linear and quadratic terms as:

$$i_{\mathrm{D}} = \mu_n C_{\mathrm{ox}} \frac{W}{L} \left( (v_{\mathrm{GS}} - v_{\mathrm{T}}) v_{\mathrm{DS}} - \frac{{v_{\mathrm{DS}}}^2}{2} \right) \quad (4)$$

where $\mu_n$ is the charge carrier effective mobility, $C_{\mathrm{ox}}$ is the gate oxide capacitance per unit area, gate width ($W$) and gate length ($L$) [21]. According to this equation, when the drain voltage is small, the drain current becomes a linear function of $v_{\mathrm{DS}}$:

$$i_{\mathrm{D}} = \mu_n C_{\mathrm{ox}} \frac{W}{L} (v_{\mathrm{GS}} - v_{\mathrm{T}}) v_{\mathrm{DS}}. \quad (5)$$

2) The saturation mode ($v_{\mathrm{GS}} > v_{\mathrm{T}}$, $v_{\mathrm{DS}} > (v_{\mathrm{GS}} - v_{\mathrm{T}})$), also above threshold, and since drain voltage is greater than the source voltage, it results in an increased electron dispersion and conduction through a broader channel. The drain current in saturation mode is:

$$i_{\mathrm{D}} = \mu_n C_{\mathrm{ox}} \frac{W}{L} \left[ v_{\mathrm{GS}} - v_{\mathrm{T}} \right]^2 \left[ 1 + \lambda v_{\mathrm{DS}} \right]. \quad (6)$$

The parameter $\lambda$ accounts for the impact of channel length modulation on drain current, known as the Early effect, and it is measured in inverse volts ($\mathrm{V}^{-1}$) [22]. It represents the change in drain current with respect to drain voltage due to variations in the channel length. Figure 3(b) shows the data-sheet version of input and output characteristics with the boundary between linear and saturation modes marked by the red line.

### C. Near Threshold ($v_{GS} = v_T$)

In our application, we require the MOSFET to operate at and near threshold since the high voltage across the inductor coil is achieved at the time of switch off (when gate voltage goes below threshold). Surprisingly, this region has not been thoroughly analyzed by researchers [4], [23]. Analytical solutions like the parallel-plate charge-control model and the unified charge-control model exist [24], [25], [26], yet they lack precise analytical solutions for the subthreshold or near-threshold region. For many applications, an approximate solution used in these models is [4]:

$$i_{\mathrm{D}} = 2\, i_{\mathrm{o}} \ln \left[ 1 + \frac{1}{2} \exp \left( \frac{v_{\mathrm{GS}} - v_{\mathrm{T}}}{\eta\ v_{\mathrm{Th}}} \right) \right] \quad (7)$$

where $i_0$ is the current corresponding to the minority carriers at threshold. This equation can be further expressed in terms of a variable $X$:

$$i_{\mathrm{D}} = 2 i_{\mathrm{o}} \ln \left[ 1 + \frac{X}{2} \right], \quad \text{where} \quad X = \exp \left( \frac{v_{\mathrm{GS}} - v_{\mathrm{T}}}{\eta\ v_{\mathrm{Th}}} \right). \quad (8)$$

Equation 7 can be evaluated across different regions to determine its applicability for sub-threshold, above-threshold, and near-threshold regions.

*1) Subthreshold Region:* In the subthreshold region ($v_{\mathrm{GS}} < v_{\mathrm{T}}$), where $X \ll 1$, we can approximate the exponential term for small values as:

$$\ln[1 + \frac{X}{2}] \approx \frac{X}{2} \quad \text{for small X}. \quad (9)$$

This simplifies Eq. (7):

$$i_{\mathrm{D}} \approx 2\ i_{\mathrm{o}} \left[ \frac{X}{2} \right] = i_{\mathrm{o}} \exp \left( \frac{v_{\mathrm{GS}} - v_{\mathrm{T}}}{\eta v_{\mathrm{Th}}} \right). \quad (10)$$

*2) Above-Threshold Region:* In the above-threshold region ($v_{\mathrm{GS}} > v_{\mathrm{T}}$), where $X \gg 1$, the exponential term dominates. We can approximate it as:

$$\ln \left[ 1 + \frac{X}{2} \right] \approx \ln \left[ \frac{X}{2} \right]. \quad (11)$$

and Eq. (7) simplifies to:

$$i_{\mathrm{D}} \approx 2\ i_{\mathrm{o}} \ln \left( \frac{1}{2} \right) + 2\ i_{\mathrm{o}} \frac{v_{\mathrm{GS}} - v_{\mathrm{T}}}{\eta v_{\mathrm{Th}}}, \quad (12)$$

in agreement with Eq. (3).

*3) At Threshold:* At the threshold ($v_{\mathrm{GS}} = v_{\mathrm{T}}$), we have:

$$X = 1, \quad (13)$$

so the equation becomes:

$$i_{\mathrm{D}} = 2\ i_{\mathrm{o}} \ln \left[ 1 + \frac{1}{2} \cdot 1 \right] = 2\ i_{\mathrm{o}} \ln \left( \frac{3}{2} \right). \quad (14)$$

Thus at the threshold condition, the current $i_{\mathrm{D}}$ is not equal to $i_{\mathrm{o}}$.

Equation (7) is suitable for both above and below the threshold regions but not near the threshold region, as $i_{\mathrm{D}}$ is not equal to the initial current at the threshold point [27], [28], [29]. All analytical approaches available are designed for lower power and small-signal MOSFETs. But no analytical model have been developed for power MOSFETs. We initially tried to use Eq. (7) to fit the data points of the measured drain current versus gate voltage for our power MOSFET, but failed. Thus we modified the drain current equation to read:

$$i_{\mathrm{D}} = \frac{i_{\mathrm{o}}}{\ln 2} \ln \left( 1 + \left[ \exp \left( \frac{v_{\mathrm{GS}} - v_{\mathrm{T}}}{\eta\ v_{\mathrm{Th}}} \right) \right]^p \right) \quad (15)$$

This equation can be further expressed in terms of a variable $X$:

$$i_{\mathrm{D}} = \frac{i_{\mathrm{o}}}{\ln 2} \ln[1 + X^p], \text{where } X = \exp \left( \frac{v_{\mathrm{GS}} - v_{\mathrm{T}}}{\eta\ v_{\mathrm{Th}}} \right). \quad (16)$$

Where, we have introduced a new parameter, the exponent $p$, and replaced the factor 2 in Eq. (7) with $\frac{1}{\ln 2}$ for reasons that will be explained in Section IV.

Figure 4(a) illustrates the failed curve fit using Eq. (7), while Fig. 4(b) demonstrates the successful fit achieved by employing the modified equation (15), which aligns much better with the data points (black dotted points).

IEEE Proof

IEEE Proof

## III. Methodology

The following summarizes the steps we took to develop the MOSFET MATLAB model:

1) Development of the drain-source current equation, $i_{L_{\text{fit}}}$: No equation or expression determines the drain-source current at all the MOSFET regions (subthreshold, at the threshold, above-threshold). So we modified an existing equation used in the literature [27] to fit experimental results as shown Eq. 15.
2) Computing the resistance of the MOSFET: After developing an equation for the current in step 1, the next step is to find the MOSFET drain-source voltage equation. To achieve this, experimental data of $v_{\text{DS}}$ (drain-source voltage), $v_{\text{GS}}$ (gate source voltage), and $i_{\text{L}}$ (TMS coil current) is utilized. Curve fitting is employed on the graph of $v_{\text{DS}}$ versus $v_{\text{GS}}$ to obtain the $v_{\text{DSfit}}$ equation. Curve fitting involves creating a mathematical function or curve that best fits the series of data points obtained from plotting $v_{\text{DS}}$ versus $v_{\text{GS}}$. With the $v_{\text{DSfit}}$ equation in hand, the $r_{\text{DS}_{\text{fit}}}$ of the MOSFET can be determined by:
$$r_{\text{DS}_{\text{fit}}} = \frac{v_{\text{DS}_{\text{fit}}}(v_{\text{GS}})}{i_{\text{L}_{\text{fit}}}(v_{\text{GS}})} \tag{17}$$
3) MATLAB model: Now we can use this $r_{\text{DS}_{\text{fit}}}$ in the differential Equation 2 as:
$$\frac{di_{\text{L}}}{dt} = \frac{1}{L}\left[v_{\text{C}} - (r_{\text{L}} + r_{\text{C}} + r_{\text{DS}_{\text{fit}}}(v_{\text{GS}}))i_{\text{L}}\right] \tag{18}$$
and solve it using any solver available in MATLAB for a given $v_{\text{GS}}(t)$ profile. We have used `ode15s` to obtain good output results depending on the input gate voltage. We have chosen the MATLAB platform for simulation instead of other options because the need for precise characterization of the MOSFET, specifically the IXFK120N65×2, used in the experiment. As the circuit performance depends on the MOSFET turn-off behavior, relying solely on the on-resistance provided in the data sheet or MOSFET models in simulation software such as SPICE would not be adequate. Therefore, we have chosen to calculate the resistance of the particular MOSFET at every instant using the experimental data we have. Furthermore, there is a gap in the available literature, as there was no common drain-source current equation that could be used in all regions. Hence, we had to develop a new equation.

## IV. Discussion of Model

We now explain the introduction of the $\ln 2$ divisor and the exponent $p$ in Eq. (15). It is critically important to note that $p$ is itself a function of $(v_{\text{GS}} - v_{\text{T}})$, as shown by the fitting in the next section.

### A. Subthreshold

In the subthreshold region ($v_{\text{GS}} < v_{\text{T}}$), where $X \ll 1$, we set $p = 1$ (this is the maximum value for the $p$ to capture the exponential characteristic of the subthreshold regime):
$$i_{\text{D}} = \frac{i_{\text{o}}}{\ln 2}\ln[1 + X], \tag{19}$$
and using
$$\ln[1 + X] \approx X \quad \text{for small X}$$
we obtain
$$i_{\text{D}} \approx \frac{i_{\text{o}}}{\ln 2}\exp\left(\frac{v_{\text{GS}} - v_{\text{T}}}{\eta\ v_{\text{Th}}}\right). \tag{20}$$
matching the Eq. (3), exponential form expected for MOSFETs.

### B. Above Threshold

In the above-threshold region ($v_{\text{GS}} > v_{\text{T}}$) where $X \gg 1$, we use $p \approx 0.2$ (the value of $p$ reduces from below-threshold to above-threshold as we need the current curve to change from exponential to linear), $i_{\text{D}}$ becomes a linear equation:
$$i_{\text{D}} = \frac{i_{\text{o}}}{\ln 2}\ln[1 + X^p] \tag{21}$$
and using
$$\ln[1 + X^p] \approx \ln X^p \quad \text{for large } X^p$$
we obtain
$$\begin{aligned} i_{\text{D}} &= \frac{i_{\text{o}}}{\ln 2}\ln[X^p] = \frac{i_{\text{o}}}{\ln 2}\ln\left[\exp\left(\frac{v_{\text{GS}} - v_{\text{T}}}{\eta\ v_{\text{Th}}}\right)\right]^p \\ &= p\frac{i_{\text{o}}}{\ln 2}\left(\frac{v_{\text{GS}} - v_{\text{T}}}{\eta\ v_{\text{Th}}}\right) \end{aligned} \tag{22}$$
Equation (15) requires a gate-voltage dependent variable $p$ to capture the transition from subthreshold to above-threshold behavior.

### C. At Threshold

At threshold, when $v_{\text{GS}} = v_T$, $X^p = 1$ for any value of $p$
$$i_{\text{D}} = \frac{i_{\text{o}}}{\ln 2}\ln[1 + X^p] = i_{\text{o}} \tag{23}$$
The modified term (ln 2) was added in Eq. (15), so that at threshold $i_{\text{D}}$ should be equal to $i_0$.

The exponent $p$ is defined by a tanh function of MOSFET gate voltage,
$$p = \frac{1}{2}\left(p_1 + p_2 + (p_2 - p_1)\tanh\left(\frac{v_{\text{GS}} - v_{\text{T}}}{\eta\ v_{\text{TH}}}\right)\right). \tag{24}$$
By modifying the Eq. 7, we achieve a successful fit that aligns with the subthreshold, at threshold, and above threshold regions. This approach treats the MOSFET as a variable resistance governed solely by the gate-source voltage, simplifying the analysis compared to treating the MOSFET as a switch. Moreover, it indirectly incorporates the influence of drain-source voltage on the resistance, thereby accounting for its effect in the model.

The crucial aspect of our application revolves around understanding MOSFET characteristics during turn-off, particularly the voltage across and current through the inductor as the MOSFET transitions to its non-conducting state. This necessitates a robust equation that accurately models behavior below, near and above threshold. Through analysis of experimental data, we derived the new equation (Eq. 15) to model high-power MOSFET behavior, thus addressing the limitations of existing analytical approaches.

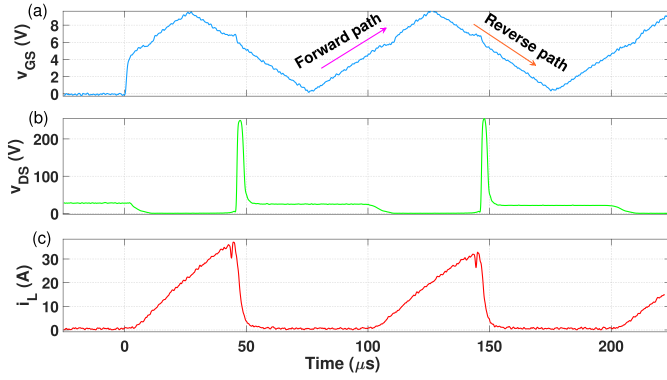


Fig. 5. (a) Gate voltage with forward path (0 to 10 V) and reverse path (10 V to 0) marked (the triangular wave is not captured for the initial 25 $\mu$s due to configuration of the triggering mechanism in the oscilloscope); (b) measured drain-source voltage and (c) coil current from the experimental setup used for the MOSFET model (To correct for current probe delay, we advanced the measured current trace by 3 $\mu$s prior to plotting).

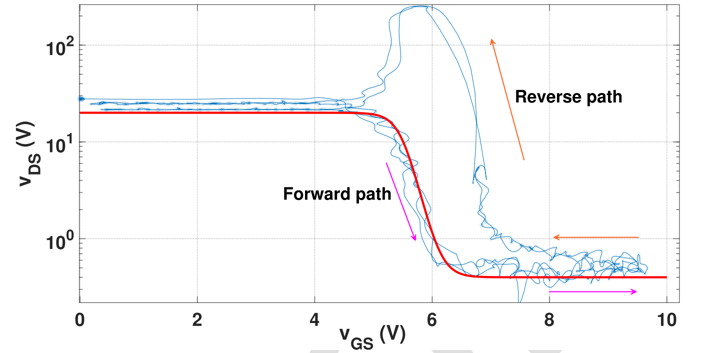


Fig. 6. Drain-source voltage versus gate voltage of the experimental result (blue). Red colored curve shows the modeled drain-source voltage fitted curve in the forward path using Eq. (25).

TABLE I
PARAMETERS AND THEIR VALUES USED FOR CURVE FITTING EQUATIONS

| Measured parameters | Symbol | Values |
|---|---|---|
| Resistance of inductor | $r_{\mathrm{L}}$ | 0.22 Ω |
| Inductance | $L$ | 0.22 $\mu$H |
| Internal resistance of $C_1$ | $r_{\mathrm{C}}$ | 0.22 Ω |
| Initial voltage of $C_1$ | $v_{\mathrm{C}}(0)$ | 30 V |
| Thermal voltage | $v_{\mathrm{TH}}$ | 26 mV |
| Threshold voltage | $v_{\mathrm{T}}$ | 6.0 V |
| Fitting parameters used in Equations | | |
| $v_{\mathrm{DS_{fit}}}$ Eq. (25) | $D_1, D_2, \eta_1$ | 20, 0.4, 12 |
| $i_{\mathrm{D}}$ Eq. (15) | $i_0, \eta$ | 8, 16 |
| $p_{\mathrm{fit}}$ Eq. (26) | $p_1, p_2, \eta_2$ | 1, 0.13, 10 |

402 ## V. COMPUTING THE RESISTANCE OF THE MOSFET

403 Now that the drain-source current equation that accurately 404 fits the experimental data is developed, the next step is to 405 determine the resistance of the MOSFET. To do so, the voltage 406 fit equation is also required. Experimental data is utilized 407 to understand the MOSFET behavior in the circuit, observing 408 how the drain current and drain-source voltage vary with 409 gate voltage. We now describe the method used to obtain 410 both voltage and current fits, which allow us to calculate the 411 resistance fit.

412 ### A. Voltage Fit

413 In our attempt to model the MOSFET S1 (Fig. 2) as a 414 nonlinear resistance, our goal is to calculate the instantaneous 415 dynamic resistance of the MOSFET at every instant throughout 416 the oscillatory cycle. To do this, we measured $v_{\mathrm{DS}}$ and $i_{\mathrm{D}}$ from 417 the experimental setup using a triangle gate voltage as input.

418 Figure 5 shows the experimental drain-source voltage ($v_{\mathrm{DS}}$) 419 and coil current ($i_{\mathrm{L}}$) (equal to drain current $i_{\mathrm{D}}$) for a 420 triangular gate voltage. We then plotted $v_{\mathrm{DS}}$ against $v_{\mathrm{GS}}$ 421 using the experimental data points (blue dots) as shown in 422 Fig 6. Here, only the forward path is modeled, which was 423 sufficient for the analysis. Additionally, the forward path varies 424 from 0 to 10 V, which covers the full range of gate voltage used 425 in the experiment. By analyzing the trajectory of the transfer 426 characteristics (blue dots in Fig. 6), we found that it follows 427 a hyperbolic tangent path since it has both upper and lower 428 limit values. Therefore, we used the equation:

429 $$v_{\mathrm{DS_{fit}}} = \frac{1}{2}\left(D_1 + D_2 + (D_2 - D_1)\tanh\left(\frac{v_{\mathrm{GS}} - v_{\mathrm{T}}}{\eta_1\ v_{\mathrm{TH}}}\right)\right) \quad (25)$$

430 The parameters used in curve fitting are provided in Table I.

431 ### B. Current Fit

432 From the experimental data of Fig. 5, the current versus 433 gate voltage graph is illustrated in Fig. 8(a) with black dots, 434 and fitted using Eq. (15). Typically, small-signal MOSFETs 435 exhibit an $\eta$ value ranging from 1 to 2. However, in this analysis, we selected the $\eta$ values listed in Table I to achieve 436 a more accurate fit, with $\eta$ being treated as a fitting parameter. 437 Choosing $\eta$ values greater than 1 is required to attain a better 438 alignment with the experimental data, particularly given the 439 specific behavior of power MOSFETs. 440

We use $p$ as a function of $(v_{\mathrm{GS}} - v_{\mathrm{T}})$, fitted to experimental 441 data. Specifically the exponent of Eq. (15) is given by 442 $p = p_{\mathrm{fit}}(v_{\mathrm{GS}} - v_{\mathrm{T}})$ where 443

$$p_{\mathrm{fit}}(v_{\mathrm{GS}} - v_{\mathrm{T}}) = \frac{1}{2}\left(p_1 + p_2 + (p_2 - p_1)\tanh\left(\frac{v_{\mathrm{GS}} - v_{\mathrm{T}}}{\eta_2\ v_{\mathrm{TH}}}\right)\right) \quad (26)$$ 444 445

The variation of $p_{\mathrm{fit}}$ against the gate voltage is shown in Fig. 7. 446

### C. Resistance Fit 447

Once we achieve an accurate fit for drain-source voltage 448 and drain current, we can compute the MOSFET resistance as 449

IEEE Proof

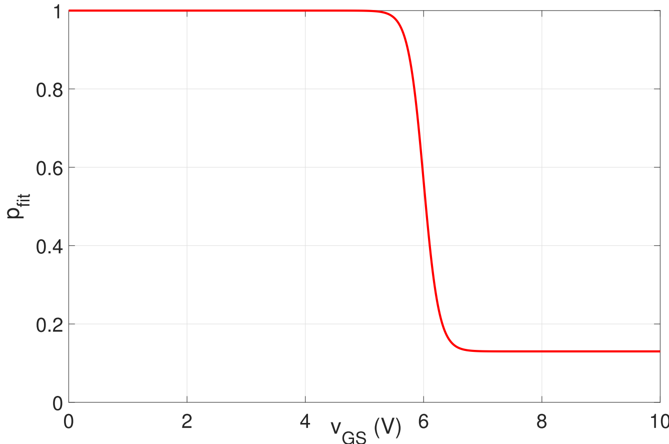


Fig. 7. Variation of exponent $p_{\text{fit}}$ with respect to the gate-source voltage ($v_{\text{GS}}$).

the ratio of voltage to current:

$$r_{\text{DS}_{\text{fit}}} = \frac{v_{\text{DS}_{\text{fit}}}}{i_{\text{L}_{\text{fit}}}} \tag{27}$$

$$= \frac{\frac{1}{2}\left(D_1 + D_2 + (D_2 - D_1)\tanh\left(\frac{v_{\text{GS}} - v_{\text{T}}}{\eta_1 \ v_{\text{TH}}}\right)\right)}{\frac{i_{\text{o}}}{\ln 2}\ln\left(1 + \left[\exp\left(\frac{v_{\text{GS}} - v_{\text{T}}}{\eta \ v_{\text{TH}}}\right)\right]^{p_{\text{fit}}}\right)} \tag{28}$$

The MOSFET is now modeled as a resistive element whose drain-source resistance $r_{\text{DS}}$ is a nonlinear function of $v_{\text{GS}}$ only,

$$r_{\text{DS}_{\text{fit}}} = f(v_{\text{GS}}) \tag{29}$$

Figure 8 shows fitting curves for current and resistance. The 3D plot in Fig. 9 illustrates the relationship between gate-source voltage, drain-source voltage, and drain current (top panel) or resistance (bottom panel).

## VI. Modeling the RLC Circuit With Time-Varying MOSFET Resistance- MATLAB Solution

With the knowledge of the time-varying MOSFET resistance, we can model the RLC circuit using a first-order differential equation. This approach allows us to establish a dynamic MOSFET description grounded in experimental data. Such a model serves as a versatile tool that encapsulates MOSFET dynamics and allows prediction of the circuit output for arbitrary input voltage waveforms applied to MOSFET gate.

Once fitting parameters for the MOSFET voltage, current, and resistance equations have been obtained, the next step is to develop a simulation model that solves the MOSFET-controlled RLC circuit shown in Figure 2. The MOSFET is treated as a variable resistance $r_{\text{DS}_{\text{fit}}}$. The circuit differential equation is:

$$\frac{di}{dt} = \frac{1}{L}\left[v_{\text{C}} - \left(r_{\text{L}} + r_{\text{C}} + r_{\text{DS}_{\text{fit}}}(v_{\text{GS}})\right)i\right] \tag{30}$$

where $r_{\text{L}}, r_{\text{C}}, v_{\text{C}}$ and $L$ are given in Table I, and $r_{\text{DS}_{\text{fit}}}(v_{\text{GS}})$ is given in Eq. (27). Any $v_{\text{GS}}(t)$ waveform can be used to test the circuit. Here we use a triangular gate voltage generated by the `pulstran` MATLAB function to match the experimental setup shown in Fig. 5.

In this MATLAB model, Euler's method was initially used to solve the differential equations for capacitor voltage and loop current but was later replaced by the more robust `ode15s`. Euler's method, while simple, often struggles with accuracy and stability, especially in 'stiff' systems where variables change at different rates. `ode15s`, a variable-order solver, dynamically adjusts the time step for better error control and is more suited for handling the stiffness of the equations describing the MOSFET-controlled RLC circuit. While MATLAB offers a range of ODE solvers, `ode15s` proved to be the most effective for this system, delivering accurate results that closely match the experimental values.

We have implemented the simulation to replicate oscilloscope readings, where the time base resolution determines the displayed output. Using the `ode15` solver, a resolution of 0.04 $\mu$s corresponds to a total simulation duration of 0.4 ms, while a resolution of 0.2 $\mu$s allows viewing five output cycles over 1.6 ms. We observed that the Euler solver performs effectively only at smaller time base resolutions and struggles at higher resolutions where more than two cycles need to be visualized.

The current probe used in the experiment has a bandwidth of DC-100 kHz, which leads to a slow response time. In contrast, the oscilloscope used for $v_{\text{L}}(t)$ voltage measurements, has a much higher bandwidth of 0-10 MHz. To correct for current probe delay, we advanced the measured current trace by 3 $\mu$s prior to plotting (Fig. 5). This leftwards timing offset was also applied to the current traces displayed in MATLAB plots of Figures 10(a) and 11(a). Figure 10(a) shows a good match between experimental measurements and MATLAB model predictions for a triangular gate input voltage. Figure 10(b) shows the oscilloscope capture results of the same 50% symmetry gate voltage input used in simulation.

MATLAB simulations produce a perfect gate waveform without any distortion. However, in the experimental setup, the gate waveform exhibits minor distortions caused by the 8-bit quantization noise in digital oscilloscope captures. In Figure 10, the leading edge of the gate voltage shows a step discontinuity instead of the expected smooth voltage ramp. This discrepancy arises because the initial 25 $\mu$s of the triangular wave is not captured accurately due to the oscilloscope triggering configuration. However, focusing on the second pulse, we observe a good alignment between the simulation results and the circuit measurements. Since we have not modeled the charging and discharging of the gate capacitance, this process causes a small blips (black circle) at the threshold voltage of the gate voltage, as shown in Fig. 10. These small imperfections can affect the current and voltage waveforms, making them slightly less precise compared to the ideal simulations. Despite these minor differences, the experimental waveforms match the MATLAB-generated output, confirming that the curve-fitting equations have successfully captured the nonlinear resistance behavior of the MOSFET.

## VII. Validation

As a test of the simulation equations, we replaced the triangular gate voltage with a 10 kHz 10 $V_{\text{pp}}$ sinusoidal signal, but modeled with the same parameters as the triangle waveform we compared the output from the `ode15s` solver

IEEE Proof

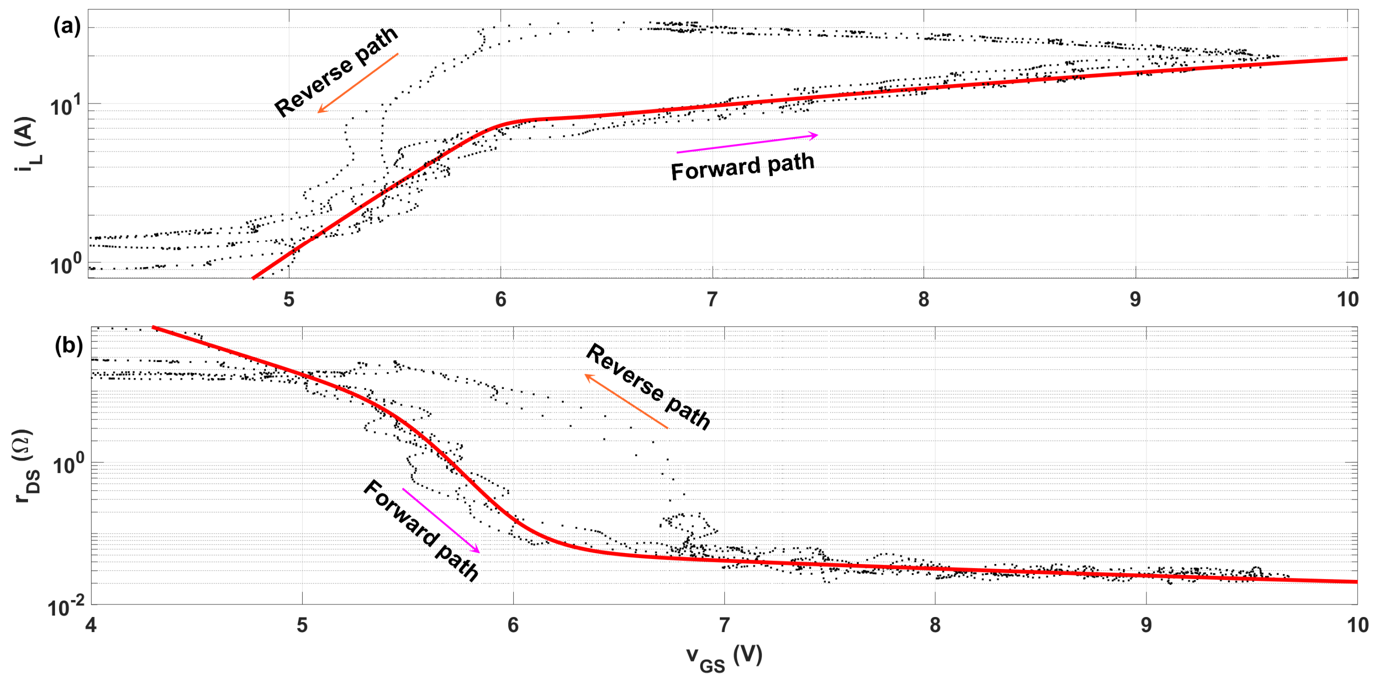


Fig. 8. (a) Transfer characteristics with fitted current curve (red line) and measured data (black dots) using Eq. (15); (b) drain-source resistance with fitted drain-source resistance curve using Eq. (27).

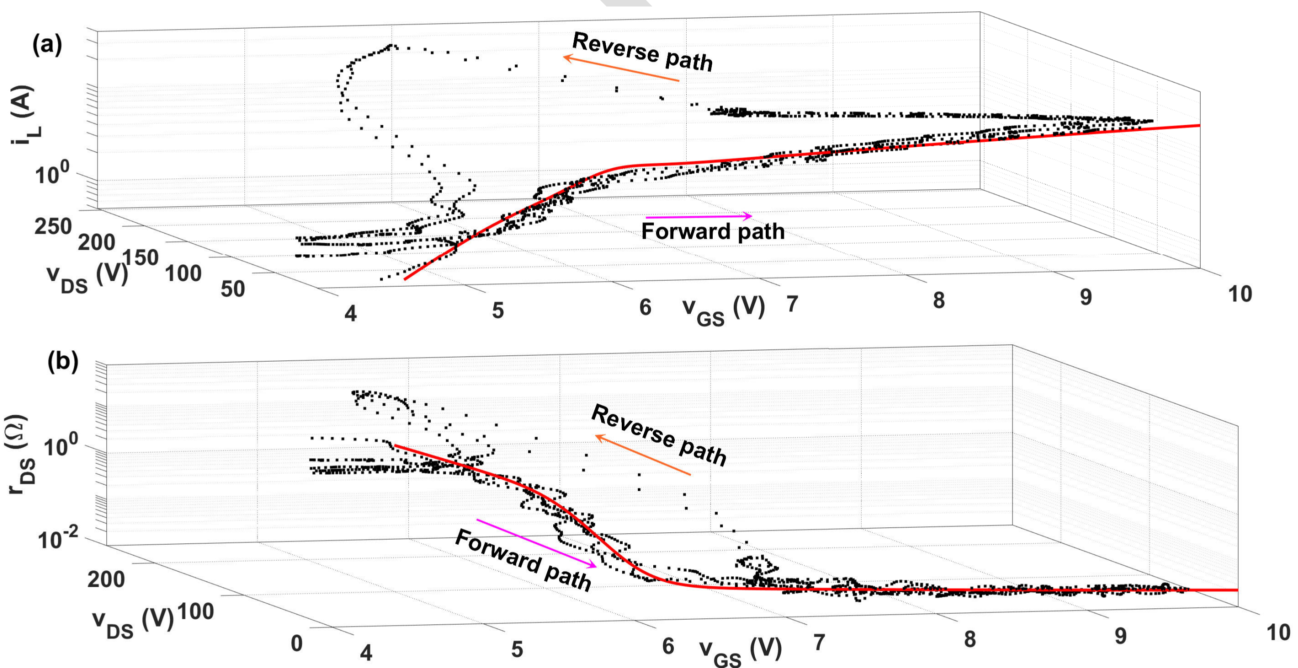


Fig. 9. Three dimensional view of the output characteristic of the MOSFET and dynamic resistance curve; (a) The measured output characteristic is shown in black dots, and the red curve shows the fitted drain-source voltage in the forward path; (b) black dots show the dynamic characteristic and, the red curve shows the fitted drain-source resistance.

539 with experimental measurements. Figure 11(a) superimposes 540 the simulation predictions against experimental measurements 541 from the oscilloscope capture shown in Fig. 11(b). It is 542 interesting to observe that the output current and voltage 543 waveforms are surprisingly insensitive to the shape (triangular 544 or sinusoidal) of the input gate voltage drive signal. This is 545 because the high voltage occurs near the threshold region primarily during turn-off, as the inductor coil only stores 546 energy at that point. In both sinusoidal and triangular 547 waveforms, the slope/points near the turn-off point around 548 the threshold region is similar, resulting in comparable output 549 behavior. 550

Figure 12 presents the experimental and MATLAB results 551 for the quadrilateral gate voltage waveform. The results 552

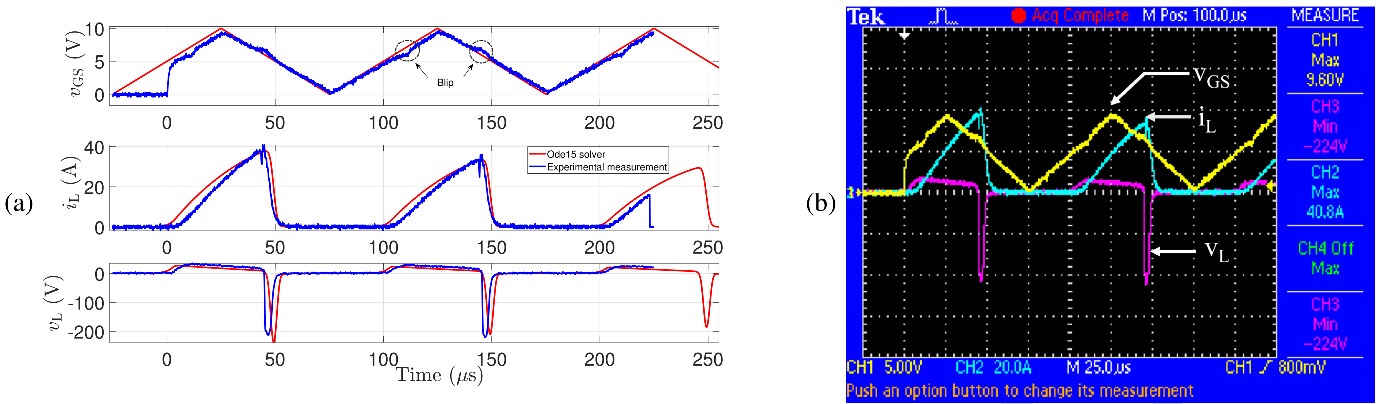


Fig. 10. Comparison of `ode15s` solver solution of the differential equation with the measured experimental values. The experimental measurement is the MATLAB of the oscilloscope view shown in (b). Blips due to charging and discharging of gate capacitance are highlighted (black circles). Note that the triangular wave is not accurately captured for the initial 25 $\mu$s due to the configuration of the triggering mechanism in the oscilloscope; (b) oscilloscope measurement of gate voltage (yellow), output coil voltage (magenta) and coil current (blue).

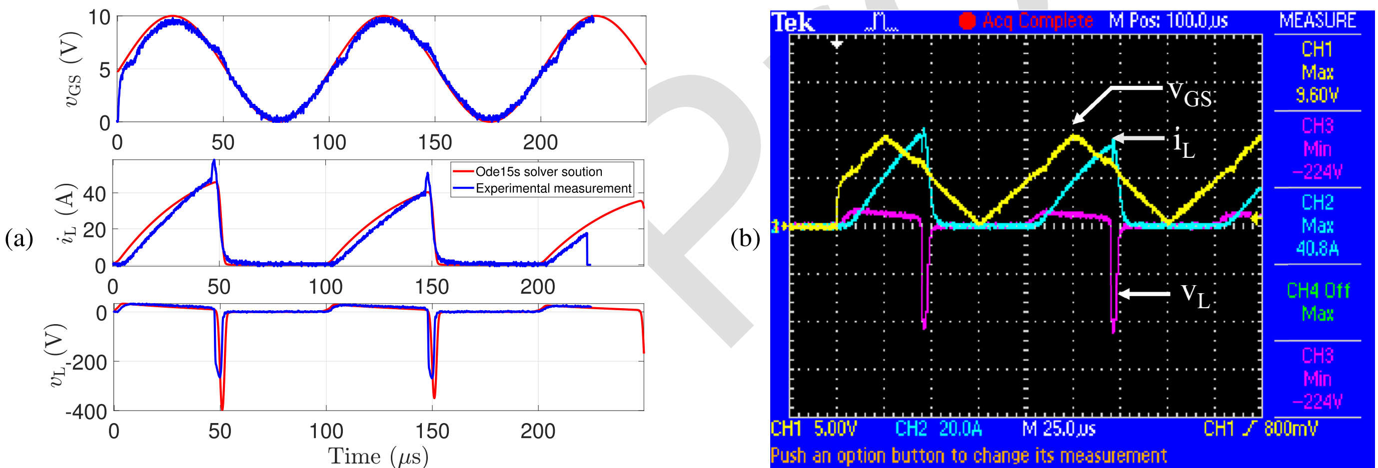


Fig. 11. (a) `ode15s` Solver solution of the differential equation (red) and experimental results (blue) with sinusoidal gate voltage input; (b) Oscilloscope measurement of sinusoidal gate voltage (yellow), output coil voltage (magenta) and coil current (blue).

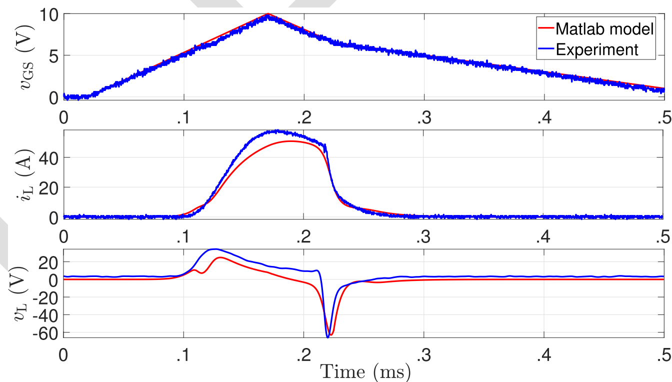


Fig. 12. Verification of experimental and MATLAB data with a quadrilateral gate voltage of 10 V amplitude.

indicate a good match between the TMS current and voltage pulses observed in the experimental setup and those from the MATLAB simulations.

## VIII. DISCUSSION

This approach to MOSFET modeling offers two key advantages. Firstly, by incorporating a comprehensive mathematical model of MOSFET behavior, simulation results provide a good match to the real-world scenarios. Secondly, the flexibility of the code allows for easy modification and adaptation to different MOSFET specifications or circuit configurations. Overall, this code segment serves as a robust tool for analyzing MOSFETs-driven RLC circuits, enabling researchers to gain insights into circuit performance and behavior under varying conditions.

However, our approach is carried out in the context of an RLC circuit. Use of Equations (27)-(28) implicitly assumes particular voltage $v_{DS}$ dynamics, and would likely need modifications for a different context. Here we have curve fitted with the parameter range that we got from the experimental data and also by looking the pattern. In contrast, variation of $i_{DS}$ with $v_{GS}$ near threshold is likely to be more robust, approximately independent of $v_{DS}$ as shown in Fig. 3(b). Although we have not yet performed reverse path-curve fitting, Figures 8 and 9 shows a hysteresis separation from the forward path; we believe it is closely related to the gate capacitance charge and discharge dynamics [30]. Despite focusing solely on the forward path from 0 to 10 V, the model still offers a reliable prediction of the output compared to the experimental results. This accuracy can be attributed to the similarity in

shape between the forward and reverse paths in the resistance plot shown in Figure 8, despite a time shift. Consequently, even without explicitly modeling the reverse path, the negative phase of the voltage in the simulation aligns closely with the experimental results.

During experimental data collection, several measurement challenges were encountered. The oscilloscope resolution made it difficult to capture the full range of data with the maximum number of points for both high and low voltage levels. When using a 100X probe, the minimum voltage values lacked accuracy. To address this, two probes were employed: a 100X probe for higher voltage levels and a 10X probe for lower voltage levels. The data from both probes were then combined in the MATLAB model.

Additionally, the resolution of the current probe and the oscilloscope differed, and we were unable to calibrate the zero-current setting on the probe. As a result, the initial inductor current values ($i_{\mathrm{L}}$) were not zero or very small, as expected. These imperfections will be addressed in the next stage of the model, where the gate capacitance will be considered. The energy dissipated and power delivered during the tests were lower than the rated values specified in the datasheet. Additionally, the MOSFET did not heat up during testing, indicating minimal thermal stress. As a result, the temperature effect has not been considered in the current analysis.

Existing studies on SiC MOSFET modeling, such as those by Tornello [9], Ferretti [10], and Wang [12], emphasize datasheet-based methods, lookup tables, and linear analyses without considering switching transients. However, they often overlook internal variations like dynamic resistance changes. Our approach addresses this gap by modeling the MOSFET as a dynamically varying resistor, considering smoothing phase transition between the sub threshold and above threshold region rather than piecewise analysis offering deeper insights into device behavior and predicting the output.

## IX. Conclusion

The development of the analytical model for nonlinear MOSFET dynamics faced several challenges, including limited data from datasheets, unexpected experimental observations, and measurement difficulties. Despite these hurdles, the model was successfully refined to accurately predict system behavior. The neglect of gate capacitance effects, although simplifying the model, did not significantly impact the accuracy of the results, which closely matched experimental data. The complexity of modeling MOSFET dynamics in the RLC circuit became evident, particularly when simulation tools like Proteus failed to replicate real-world results. However, by fine-tuning resistance, threshold values, and utilizing curve fitting based on a physical descriptions of the near threshold region, the MATLAB model provided reliable predictions. This work offers a strong physical foundation for power MOSFET modeling, allowing for more accurate simulations with minimal additional experimentation.

This study can be significant because, in the existing literature, there are primarily Simulink block models or subthreshold equations, with no dedicated equation available to cover the full operating range of a MOSFET. Our approach can serve as a valuable tool for other researchers to evaluate circuits where the MOSFET is treated as a dynamically varying element.

## X. Future Work

In future work, we are working to incorporate stray inductance and capacitance effects into the model, as these factors play a critical role in circuit performance. While this study focuses on the initial development stage, we recognize the importance of addressing these elements and will include them in the next phase.

## Acknowledgment

The authors gratefully acknowledge the University of Waikato Doctoral Scholarship for the research support.

## References

[1] Z. Feng, A. Berry, P. Ellis, and W. Lawson, "SPICE models for predicting EMC performance of a MOSFET based half-bridge configuration," in *Proc. IEEE 1st Int. Power Electron. Appl. Symp. (PEAS)*, Nov. 2021, pp. 1–5.

[2] D. G. A. Neto, G. Maranhão, M. C. Schneider, and C. Galup-Montoro, "A design-oriented single-piece short-channel MOSFET model," in *Proc. IEEE Int. Symp. Circuits Syst. (ISCAS)*, May 2024, pp. 1–5, doi: 10.1109/ISCAS58744.2024.10558311.

[3] K. Lee, M. Shur, T. A. Fjeldly, and T. Ytterdal, *Semiconductor Device Modeling for VLSI*. Upper Saddle River, NJ, USA: Prentice-Hall, 1993.

[4] M. Shur, T. A. Fjeldly, T. Ytterdal, and K. Lee, "Unified MOSFET model," *Solid-State Electron.*, vol. 35, no. 12, pp. 1795–1802, Dec. 1992.

[5] J. Xie et al., "An accurate and effective spice model of 6.5kV SiC MOSFET with parasitic parameters analysis in medium-voltage power module," in *Proc. IEEE 10th Int. Power Electron. Motion Control Conf. (IPEMC-ECCE Asia)*, May 2024, pp. 3487–3492, doi: 10.1109/IPEMC-ECCEASIA60879.2024.10567836.

[6] F. Wang, S. Kher, T. Fichtner, and J. Aurich, "A new power MOSFET model and an easy to use characterization tool using device datasheet," in *Proc. IEEE 14th Workshop Control Model. Power Electron. (COMPEL)*, Jun. 2013, pp. 1–5, doi: 10.1109/COMPEL.2013.6626471.

[7] M. Mudholkar, M. Saadeh, and H. A. Mantooth, "A datasheet driven power MOSFET model and parameter extraction procedure for 1200 V, 20A SiC MOSFETs," in *Proc. 14th Eur. Conf. Power Electron. Appl.*, Aug. 2011, pp. 1–10.

[8] A. Ghulam et al., "Accurate & complete behaviourial SPICE modelling of commercial SiC power MOSFET OF 1200 V, 75A," in *Proc. 25th Int. Conf. Thermal, Mech. Multi-Physics Simul. Experiments Microelectron. Microsystems (EuroSimE)*, Apr. 2024, pp. 1–4.

[9] L. D. Tornello, M. G. Spitaleri, G. Scarcella, and M. Cacciato, "An analytical model of a SiC MOSFETs in parallel configuration," in *Proc. ELEKTRO (ELEKTRO)*, May 2024, pp. 1–6.

[10] J. Ferretti, G.-P. Schiapparelli, E. Sangiorgi, and A. N. Tallarico, "SiC MOSFETs performance modeling in simulink simscape environment," in *Proc. IEEE 10th Workshop Wide Bandgap Power Devices Appl. (WiPDA)*, Dec. 2023, pp. 1–6.

[11] P. Zeng, S. Wu, Y. Luo, and X. Xiao, "Research on SiC MOSFET model based on simulink," in *Proc. 7th Int. Conf. Comput. Inf. Sci. Appl. Technol. (CISAT)*, Jul. 2024, pp. 679–682.

[12] N. Wang and J. Zhang, "Nonlinear capacitance model of SiC MOSFET considering envelope of switching trajectory," *IEEE Trans. Power Electron.*, vol. 37, no. 7, pp. 7977–7988, Jul. 2022.

[13] V. Talesara et al., "Dynamic switching of SiC power MOSFETs based on analytical subcircuit model," *IEEE Trans. Power Electron.*, vol. 35, no. 9, pp. 9680–9689, Sep. 2020.

[14] C. Wang, H. Chen, H. Wang, Z. Wang, and X. Ye, "Refined electrical modelling of power MOSFETs based on physical information," in *Proc. 5th Int. Conf. Syst. Rel. Saf. Eng. (SRSE)*, Oct. 2023, pp. 164–169.

[15] X. Yang, J. Li, Y. Ding, M. Xu, X.-F. Zhu, and J. Zhu, "Observation of transient parity-time symmetry in electronic systems," *Phys. Rev. Lett.*, vol. 128, no. 6, Feb. 2022, Art. no. 065701.

IEEE Proof

[16] Q. Liu, P. Sun, G. Peng, and X. Ma, "A semi-physical model of SiC MOSFETs for improved static characteristic," in *Proc. IEEE 7th Int. Electr. Energy Conf. (CIEEC)*, May 2024, pp. 1842–1845, doi: 10.1109/CIEEC60922.2024.10583229.

[17] Y. Mukunoki et al., "Modeling of a silicon-carbide MOSFET with focus on internal stray capacitances and inductances, and its verification," in *Proc. IEEE Appl. Power Electron. Conf. Expo. (APEC)*, Mar. 2017, pp. 2671–2677, doi: 10.1109/APEC.2017.7931076.

[18] S. Raju, N. Kularatna, and M. Wilson, "Supercapacitor based adjustable high power pulse generator for medical research applications," in *Proc. 49th Annu. Conf. IEEE Ind. Electron. Soc.*, Oct. 2023, pp. 1–6.

[19] Littelfuse. (2024). *Discrete MOSFETs N-Channel Ultra Junction IXF120N65X2 Datasheet*. Accessed: Sep. 26, 2024. [Online]. Available: https://shorturl.at/09f62

[20] P. van der Meer, A. van Staveren, and A. H. van Roermund, *Low-Power Deep Sub-Micron CMOS Logic: Sub-Threshold Current Reduction*, vol. 841. Berlin, Germany: Springer, 2004.

[21] B. J. Baliga, *Silicon RF Power MOSFETs*. Singapore: World Scientific, 2005.

[22] R. C. Jaeger, T. N. Blalock, and B. J. Blalock, *Microelectronic Circuit Design*, vol. 97. New York, NY, USA: McGraw-Hill, 1997.

[23] M. Shur and J. Singh, "Physics of semiconductor devices," *Phys. Today*, vol. 43, no. 10, pp. 98–99, doi: 10.1063/1.2810727.

[24] N. D. Arora, *MOSFET Models for VLSI Circuit Simulation: Theory and Practice*. Berlin, Germany: Springer, 2012.

[25] J. R. Brews, W. Fichtner, E. H. Nicollian, and S. M. Sze, "Generalized guide for MOSFET miniaturization," in *IEDM Tech. Dig.*, Dec. 1979, pp. 10–13.

[26] Y. H. Byun, K. Lee, and M. Shur, "Unified charge control model and subthreshold current in heterostructure field-effect transistors," *IEEE Electron Device Lett.*, vol. 11, no. 1, pp. 50–53, Jan. 1990, doi: 10.1109/55.46928.

[27] T. Ytterdal, Y. Cheng, and T. A. Fjeldly, *Device Modeling for Analog and RF CMOS Circuit Design*. Hoboken, NJ, USA: Wiley, 2003.

[28] T. A. Fjeldly and M. Shur, "Threshold voltage modeling and the subthreshold regime of operation of short-channel MOSFETs," *IEEE Trans. Electron Devices*, vol. 40, no. 1, pp. 137–145, Jan. 1993.

[29] T. A. Fjeldly, M. Shur, and T. Ytterdal, *Introduction to Device Modeling and Circuit Simulation*. Hoboken, NJ, USA: Wiley, 1997.

[30] M. Xu, X. Yang, and J. Li, "C-RC snubber optimization design for improving switching characteristics of SiC MOSFET," *IEEE Trans. Power Electron.*, vol. 37, no. 10, pp. 12005–12016, Oct. 2022, doi: 10.1109/TPEL.2022.3180387.

**Soniya Raju** (Member, IEEE) was born in Kerala, India. She received the degree (Hons.) in electrical and electronics engineering from Mahatma Gandhi University, Kerala, in 2014, and the master's degree in power electronics and drives with a specialization in power electronics application in power systems from Karunya University, Tamil Nadu, in 2016. She is currently pursuing the Ph.D. degree with The University of Waikato. She was an Assistant Professor for five years in India. Her research interests encompass a diverse range, including power electronics, circuit designing, transcranial magnetic stimulation, and supercapacitors.

**D. Alistair Steyn-Ross** received the B.Sc., M.Sc., and Ph.D. degrees in physics from the University of Waikato (UoW), Hamilton, New Zealand, in 1975, 1977, and 2002, respectively. He is currently an Associate Professor with the School of Engineering, UoW. He has supervised a substantial number of Ph.D. projects in the application of supercapacitors to renewable-energy storage and the design of robust, energy-efficient dc power supplies, and has coauthored more than 50 papers on supercapacitor-related topics. His research expertise is the application of computational physics and mathematics to the modeling of nonlinear stochastic systems during close approach to phase transition critical points.

**Marcus Wilson** received the degree (Hons.) in physics and theoretical physics from the University of Cambridge, U.K., in 1992, and the Ph.D. degree in theoretical solid state physics from the University of Bristol, U.K., in 1995. He is currently a Senior Lecturer in physics and emistry with the Te Aka Mātuatua, School of Science, The University of Waikato, Hamilton, New Zealand. He has worked in numerical modeling of physics processes in industry in U.K. and in academia in New Zealand, the latter since 2004. His research interests include electric properties and dynamics of the human brain, transcranial magnetic stimulation, and more recently batteries.

**Nihal Kularatna** (Senior Member, IEEE) received the D.Sc. degree in electronic engineering in 2015. Prior to moving to academia in New Zealand, he was the CEO of the Arthur C Clarke Institute for Modern Technologies, Sri Lanka. He is currently an Associate Professor with The University of Waikato, Hamilton, New Zealand. He is research-active in supercapacitor applications and power electronics. He has authored ten reference books and research monographs, and contributed more than 175 publications. He was a recipient of the Post Graduate Research Supervision Excellence Award from The University of Waikato in 2021. For developing supercapacitor-assisted (SCA) techniques, he won the NZ Engineering Innovator of the Year 2013 Award.

IEEE Proof